

Introducing HTDP 3.1 to transform coordinates across time and spatial reference frames

Chris Pearson · Richard Snay

Received: 29 July 2011 / Accepted: 17 January 2012
© Springer-Verlag (outside the USA) 2012

Abstract The National Geodetic Survey, an office within the National Oceanic and Atmospheric Administration, recently released version 3.1 of the Horizontal Time-Dependent Positioning (HTDP) utility for transforming coordinates across time and between spatial reference frames. HTDP 3.1 introduces improved crustal velocity models for both the contiguous United States and Alaska. The new HTDP version also introduces a model for estimating displacements associated with the magnitude 7.2 El Mayor–Cucapah earthquake of April 4, 2010. In addition, HTDP 3.1 enables its users to transform coordinates between the newly adopted International Terrestrial Reference Frame of 2008 (ITRF2008) and IGS08 reference frames and other popular reference frames, including current realizations of NAD 83 and WGS84. A more convenient format to enter a list of coordinates to be transformed has been added. Users can now also enter dates in the decimal year format as well as the month-day-year format. The new HTDP utility, explanatory material and instructions are available at <http://www.ngs.noaa.gov/TOOLS/Htdp/Htdp.shtml>.

Keywords Crustal deformation · Geodesy · Dynamic datums · NAD83

Introduction

In 1992, the National Geodetic Survey (NGS) introduced the Horizontal Time-Dependent Positioning (HTDP) software (Pearson et al. 2010) that enables users to correct positional coordinates and/or geodetic observations for the effect of crustal deformation and transforming positional coordinates and velocities between reference frames.

HTDP supports these functions by incorporating models for horizontal crustal velocities and models for the displacements associated with most major earthquakes that have occurred in the United States since 1934. Every so often, NGS releases a new version of HTDP that introduces a completely new crustal motion model or a revision of an existing model, or when additional capabilities have been added to the software utility. In March 2011, NGS released version 3.1 of HTDP, which introduces:

- An improved model for estimating horizontal velocities in western contiguous United States (CONUS). This model was obtained by combining estimated velocities, derived from repeated geodetic observations and used in previous HTDP models, with newly derived velocities estimated by UNAVCO (for sites in the Plate Boundary Observatory network), by the Southern California Earthquake Center (for sites located in California), and by NGS (for sites located in the U.S. Continuously Operating Reference Stations (CORS) network).
- A densification of HTDP's grid in central California to provide more accurate velocity estimates where the San Andreas fault experiences significant surface slip.

C. Pearson (✉)
NOAA's National Geodetic Survey, 2300 South Dirksen Pkwy,
Springfield, IL 52703, USA
e-mail: Cpearson86@aol.com

Present Address:
C. Pearson
Surveying Department, Otago University, Box 56,
Dunedin, New Zealand

R. Snay
NOAA's National Geodetic Survey (retired), 1315 E-W
Highway #8615, Silver Spring, MD 20910, USA

- A model for estimating horizontal velocities for locations in and near Alaska whose latitudes range from 55°N to 66°N and whose longitudes range from 131°W to 163°W.
- A model for estimating displacements associated with the M 7.2 El Mayor–Cucapah earthquake, which occurred in northern Baja California, Mexico on April 4, 2010. This model was developed by Dr. Yuri Fialko of the Institute of Geophysics and Planetary Physics, University of California at San Diego (Fialko pers. comm., 2010).
- An enhancement so that HTDP 3.1 users may submit batch files in a new convenient format when transforming coordinates for multiple stations across time and/or between reference frames.
- A 14-parameter transformation for converting coordinates and velocities between ITRF2008 or IGS08 and other common spatial reference frames.
- Transformations for three new geometric reference frames supported by NGS. NAD83(2011) replaces NAD83(CORS96) as the latest realization of the North American tectonic plate-fixed frame; NAD 83(PA11) replaces NAD83(PACP00) as the latest realization of the Pacific tectonic plate-fixed frame and NAD 83(MA11) replaces NAD83(MARP00) as the latest realization of the Mariana tectonic plate-fixed frame. Furthermore, these latest realizations all have a reference epoch of 2010.00, updated from 2002.0 for CORS96 and 1993.62 for MARP00 and PACP00.

Upgrading the velocity model for western CONUS

The model of the secular velocities included in HTDP is based on a DEFNODE model (McCaffrey 1995, 2002) containing over 50 blocks covering a rectangular area ranging from 100°W to 125°W in longitude and from 31°N to 49°N in latitude in the contiguous US (CONUS). Figure 1 shows the blocks covering western CONUS (McCaffrey 2005; McCaffrey et al. 2007). The velocity field of the modeled region is later sampled to produce the grid files that are incorporated in the HTDP software. The DEFNODE model contains explicit representations for major faults in western CONUS and a uniform strain rate tensor for each block. Slip rates on the faults range from over 30 mm/year for the Cascadia subduction interface and parts of the San Andreas system to near zero (generally sub 1 mm/year) for faults located in the eastern side of the modeled region. Pearson et al. (2010) present a detailed description of the geophysical results of this model.

The DEFNODE model is principally constrained by the geodetically determined horizontal velocity vectors. In

2007, there were 4,890 vectors available for this purpose. However, in the 3 years since then, a great number of new velocity data have become available, including data from the Plate Boundary Observatory (PBO) (<http://pboweb.unavco.org/?pageid=88>), velocity estimates from NGS's Multi-Year CORS study (Griffiths et al., in prep.), and the CMM4 solution (Shen et al. 2011) increasing the number of vectors to 6,292 (see Table 1 for details). Figure 1 shows the velocity vectors included in the revised DEFNODE inversion.

Data from seven regions were not included in the inversion. The data in these seven regions were excluded because the crustal deformation experienced there is dominated by volcanic processes (five cases) or postseismic processes (two cases) that cannot be modeled effectively by DEFNODE, which is a block modeling program based on elastic dislocation theory so, at present, these processes are ignored. The seven excluded regions are listed in Table 2 and shown in Fig. 1. Because we are not able to model these processes effectively, HTDP's velocity predictions might not be as accurate within the seven excluded regions.

Velocity grids contained in HTDP 3.1

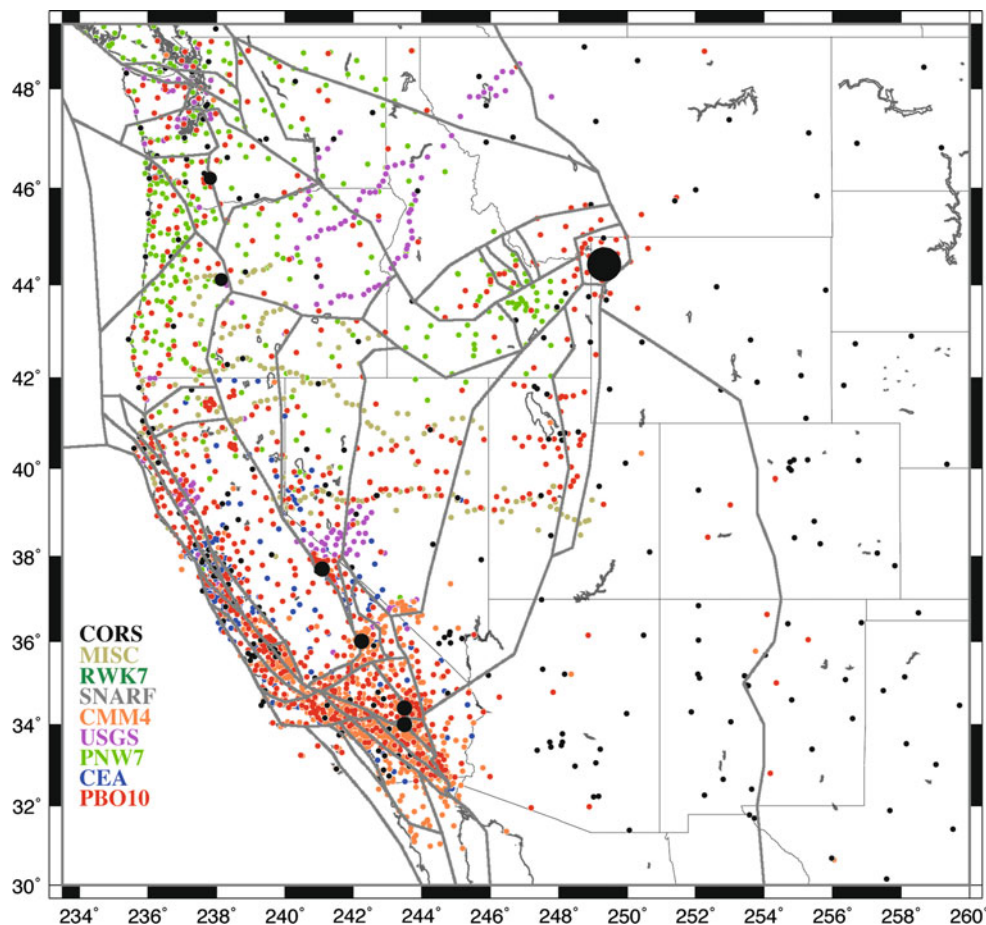
Once model parameters have been estimated with DEFNODE, these parameters can be used to predict the horizontal velocity at any point in western CONUS by running DEFNODE in its predictive (forward model) mode. HTDP uses five grid files to interpolate the secular velocities predicted by DEFNODE. These grids cover different regions with different cell sizes in order to maintain a desired level of accuracy in regions of higher velocity gradients. All of the values contained in the velocity grids are computed using parameters from a single DEFNODE inversion. Consequently, the velocity estimate of overlapping grids will match exactly at common points so continuity of the interpolated velocities across the boundary where a higher resolution grid supersedes a lower resolution one is guaranteed. Note that our bilinear interpolation procedure guarantees only zero-order continuity along and across boundaries and some inconsistency in the first and higher order derivatives of the velocity field is possible in areas where the velocity field exhibits nonlinear behavior over a spacing of the coarser grid. We reduced the possibility of this type of inconsistency by placing the boundaries between velocity grids in areas where the velocity field is approximately linear over both grid intervals. HTDP will automatically choose the most accurate grid for the point in question. Table 3 lists the velocity grids contained in HTDP 3.1, and Fig. 2 shows a visualization of the HTDP3.1 velocity field relative to NAD 83(2011).

Table 1 Data used for developing a new velocity model for western CONUS

Data set	# of vectors	RMS N mm/year	RMS E mm/year	Source
ITR08	131	0.86	0.98	Altamimi et al. (2011)
SNRF	18	0.44	0.59	SNARF website
DXB2	16	0.76	1.23	Dixon et al. (2002)
HT04	67	0.84	0.93	Hammond and Thatcher (2004)
HT05	94	1.34	1.08	Hammond and Thatcher (2005)
WILL	31	0.93	1.63	Williams et al. (2006)
CEA1	1264	1.39	1.41	California Earthquake Authority
DMEX	12	0.65	2.00	Marquez-Azua and DeMets (2003)
PBO9	1047	1.22	1.29	http://pboweb.unavco.org/
PNW7	578	0.81	0.78	McCaffrey et al. (2007), Payne et al. (2007)
USGS	299	1.27	1.40	USGS website
RWK7	770	1.30	1.23	King et al. (2007), D'Alessio et al. (2005)
CMM4	1068	1.33	1.24	Shen et al. (2011)
CORS	892	1.05	1.10	NGS CORS multiyear solution

The SNARF data from http://www.unavco.org/community_science/workinggroups_projects/snarf/snarf.html, the NGS multiyear CORS solution is a preliminary velocity estimate as of October 13, 2010 (Griffiths pers. com. 2010) and the PBO was posted as of October 2009

Fig. 1 Data used for developing a new velocity model for western CONUS with colors indicating data source. Labels refer to Table 1. MISC includes the ITR08, DXB2, HT04, HT05, WILL and DMEX data sets. The figure also shows the block boundaries used in the DEFNODE model. The seven circular regions where velocity data were excluded are shown in *black*



Because the least squares inversion program and the underlying tectonic model used for HTDP 3.1 are the same as those used for HTDP 3.0, the respective velocity grids

were expected to be similar with small improvements to reflect the extra data. However, this new version contains a significant improvement over HTDP 3.0, due to improved

Table 2 Circular regions where velocity data were excluded

Name	Center latitude deg	Center longitude deg	Radius km
Mammoth Lakes Volcanic Region	37.8	118.9	20
Coso Volcanic Field	36	117.75	20
Yellowstone Volcanic Region	44.43	110.67	50
South Sister Volcano	44.1	121.85	20
Mount St Helens Volcano	46.2	122.18	20
Landers earthquake	34	116.5	20
Landers earthquake	34	116.5	20

Table 3 Velocity grids used in HTDP 3.1

Longitude range	Latitude range	Cell spacing (min)	Grid dimensions	Region
100°–125°W	31°–49°N	15	101 × 73	Entire region
122°–125°W	40°–49°N	3.75	49 × 145	Pacific NW
119°–125°W	36°–40°N	3.75	97 × 65	Northern CA
114°–121°W	31°–36°N	3.75	113 × 81	Southern CA
120.51°–121.4°W	35.8°–36.79°N	0.6	130 × 100	Slipping San Andreas
131°–163°W	55°–66°N	15	45 × 129	Alaska

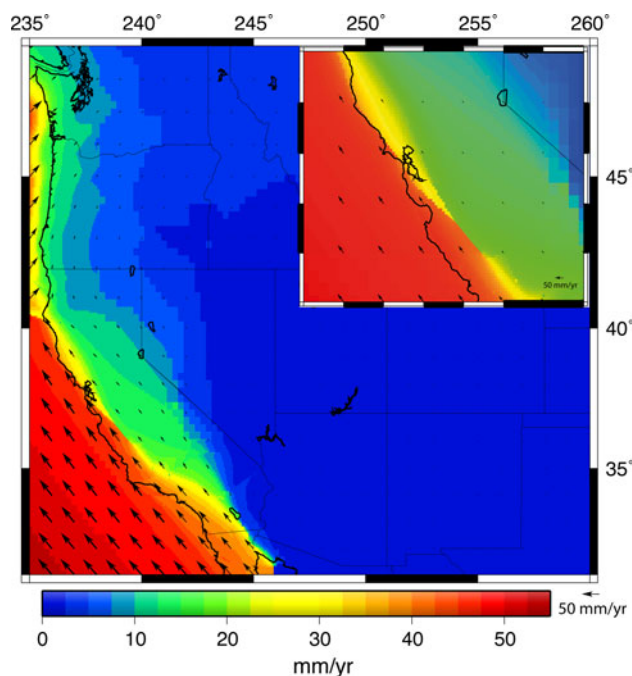


Fig. 2 Visualization of the HTDP3.1 velocity field relative to NAD 83(2011). Predicted velocities on 1 degree grid are shown in *black*. The pixel size in this figure represents the cell spacing in the HTDP velocity grid, coarse in the east where the velocities change very slowly and becoming finer in the tectonically active regions along the west coast. The *inset* provides greater detail for the velocity field in central California

handling of the creeping section of the San Andreas fault where the two sides of the fault slip past each other in opposite directions producing a spatial discontinuity in the

velocity field. This section of the fault is problematic because HTDP uses bilinear interpolation to estimate point velocities in each grid cell. The HTDP 3.0 velocity grid—with a 3.75 “by 3.75” spacing—was too coarse to follow the very sudden velocity change across this segment of the San Andreas fault. To deal with this deformation, NGS added a new velocity grid with a 0.6 “by 0.6” spacing in the vicinity of the fault. Although no grid can perfectly represent this discontinuous change in velocities, the new finer grid follows the change better. The pixel size in this figure represents the cell spacing in the HTDP velocity grid, coarse in the east where the velocities change very slowly and becoming finer in the tectonically active regions along the west coast. This figure shows a very strong velocity gradient across California south of Cape Mendocino due to the presence of the San Andreas fault. Velocities range from over 50 mm/year in the coastal regions to less than 10 mm/year in the eastern boundaries of the state. Farther north in Washington and Oregon, the velocity gradient is much more restrained because the major plate boundary fault there is the Cascadia Subduction Zone, which is located over 50 km off shore.

Test of the CONUS velocity grids

We used a set of 1,271 velocity vectors provided by the California Spatial Reference Center (Yehuda Bock 2011, pers. comm.) to validate the velocity field for western CONUS. These velocity vectors provide an independent

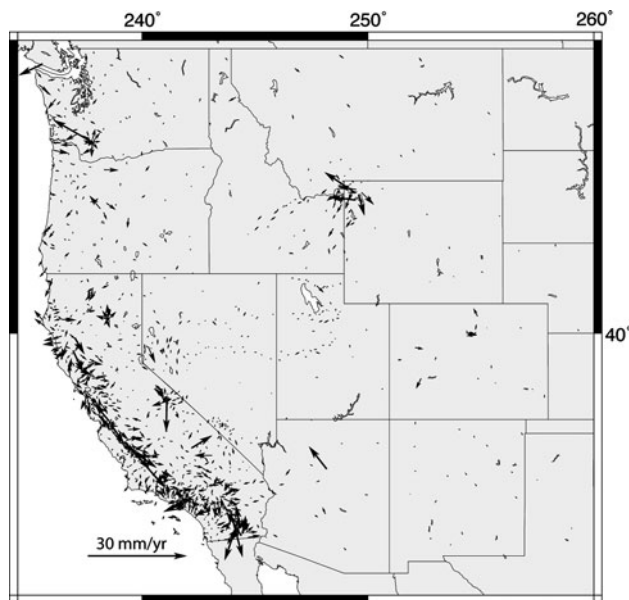


Fig. 3 Residual velocity vectors for the CSRC test points

test because they were not used as constraints during the development of our model (<http://sopac.ucsd.edu/processing/coordinates/>). Figure 3 shows the residual velocity vectors derived by comparing the measured velocities with predicted values from HTDP (Table 4).

Figure 4 shows a histogram of the azimuths of the residuals. Clearly, the azimuths are reasonably evenly distributed across all possible azimuths without a preferred direction. As a result, the misfit is probably caused by random errors and there does not seem to be any evidence of a bias.

Alaskan velocity model

HTDP 3.1 introduces a significant upgrade to the velocity model for Alaska that was encoded into HTDP 3.0. For HTDP 3.1, we started with a set of 591 geodetically derived velocity vectors from Freymueller et al. (2008), then added 23 CORS-generated velocity vectors (Griffiths et al. in prep.) and 53 PBO derived velocity vectors (<http://pboweb.unavco.org/>). These velocities are known to be affected by postseismic deformation associated with the 1964 Prince William Sound earthquake, but because the

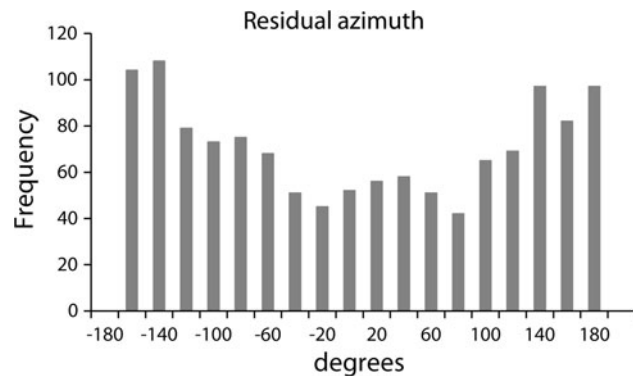


Fig. 4 Histogram of the azimuth of the residual vectors between HTDP 3.1 predicted velocities and measured velocities from the California Spatial Reference Center

postseismic deformation has reached such a mature stage and is changing slowly (Suito and Freymueller 2009), the velocities measured during the last decade can be used as an estimate of the total deformation (interseismic deformation plus the residual postseismic deformation associated with the 1964 earthquake), that is, the postseismic deformation can be treated as reasonably constant over periods of a decade. Postseismic processes from the 2002 Denali earthquake can also potentially affect the velocity estimates, but the velocity estimates from Freymueller et al. (2008) are thought to be sufficiently far from the rupture zone so that the effect will be small or because the velocity estimates utilize only pre-earthquake data. The velocity field in the Cook Inlet is also effected by a large slow slip event that occurred between 1998 and 2001 (Freymueller et al. 2008). The available velocity vectors are shown in Fig. 5. Because the DEFNODE model used for western CONUS does not extend to Alaska, we developed the velocity grid by interpolating the derived velocity vectors using bi-cubic splines. As expected, this technique works very well in central Alaska where a reasonably dense distribution of velocity determinations exists; however, not surprisingly, the technique is inadequate in regions where measurements are sparse or absent, such as the far western and eastern parts of the State and near the Gulf of Alaska. To address this problem, we added velocity constraints (calculated velocities using existing tectonic models) in areas where there were no observations. In the far south, we constrained velocities for locations in

Table 4 Comparing vector-coordinate differences between velocities from the California Spatial Reference Center with HTDP 3.1 velocities for western CONUS

	Max (mm/year)	Min (mm/year)	RMS (mm/year)	Average (mm/year)
North difference	7.42	-14.00	1.49	-0.26
East difference	12.51	-12.07	1.42	-0.03

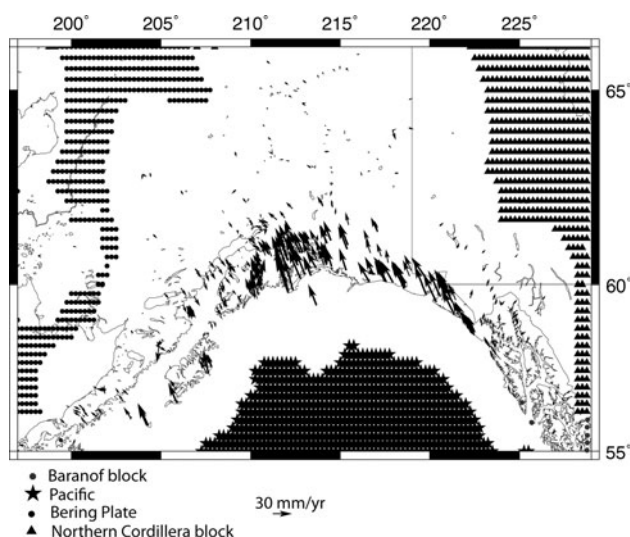


Fig. 5 NAD83 velocities and constraints used to develop the Alaska velocity grid. Other constraints are shown by various symbols shown in the *key*

the central Gulf of Alaska to the Pacific plate rate. In the far west, we used velocities from the Bering plate model proposed by Cross and Freymueller (2007, 2008); and for eastern Alaska and adjacent parts of northern British Columbia and the Yukon, we used the Baranof and Northern Cordillera block models from Elliott et al. (2010). These block motions represent only the stable interseismic velocities, in contrast to some of the measured velocities discussed above that include the combined effects of interseismic deformation plus the residual postseismic deformation associated with the 1964 earthquake. However, these velocity estimates are for areas that are located sufficiently far from the rupture zone of the 1964 earthquake, so postseismic effects would be small. Because both the Cross and Freymueller model and the Elliot et al. model were calculated in a North America-fixed frame developed using the Euler pole for North America presented by Sella et al. (2007), we used the same pole to rotate the predicted velocities for all three blocks back into the ITRF2000 reference system. These point velocity estimates and the velocity estimates from Freymueller et al. (2008) were later transformed into the ITRF2005 reference system so that all the velocities could be gridded in a common datum. The resulting grid was later transformed into ITRF2008 using a beta version of HTDP 3.1.

Alaskan velocity field

Figure 6 shows the new Alaskan velocity grid in the NAD 83 (2011) reference frame that was designed so that points in stable North America have zero horizontal velocity on

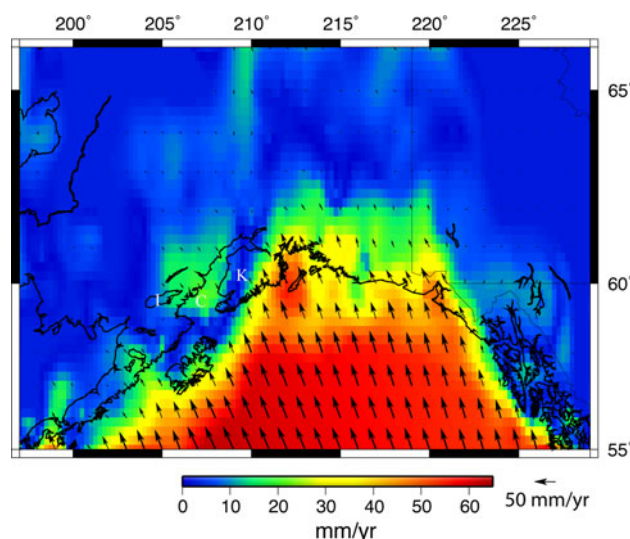


Fig. 6 Visualization of the HTDP 3.1 Alaskan velocity grid relative to NAD 83 (2011). Predicted velocities on 1 degree grid are shown in *black*. The location of the Lake Iliamna is labeled by I, the Cook Inlet by C, and the Kenai Peninsula by K

average (Snay 2003; Snay and Soler 2000). In this reference frame, most of the Alaskan mainland is not moving significantly with the exception of a zone of between 200 and 300 km in width along the southern coast of central Alaska, which represents the transition zone between the Pacific and North America plates. The region extending from eastern Lake Iliamna through the lower part of Cook Inlet and the southeast edge of the Kenai Peninsula (appearing in green in Fig. 6) is characterized by anomalous trenchward velocities. These are probably related to the postseismic relaxation associated with the 1964 Prince William Sound earthquake (Suito and Freymueller 2009) and the 1998–2001 slow slip event.

Test of the Alaskan model

We tested the velocity model using a set of 100 velocity vectors from the recent PBO solutions (Freymueller pers. com 2011). Because about half of these velocities are for stations that had not participated in determining our velocity grid due to insufficient data while the other half have an extra 2 years of data, they can be considered to be an independent test data set. Figure 7 presents a map of the HTDP 3.1 residuals in Alaska showing both the older data used to develop the model (in black) and the 100 independent test data points (in red). For comparison, Fig. 8 presents similar plot (using just the Freymueller velocities) for the HTDP 3.0 residuals in Alaska. The HTDP 3.1 model does a much better job of matching the observed velocities and avoids the very strong systematic residuals that the HTDP 3.0 model has in the coastal region of Alaska.

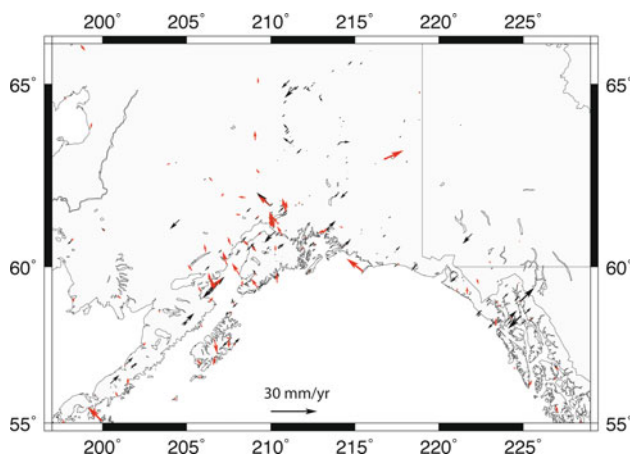


Fig. 7 Residuals for the HTDP 3.1 velocity grid of Alaska. Residuals from the data used to develop the model are shown in *black*, and the 100 independent test data points are shown in *red*

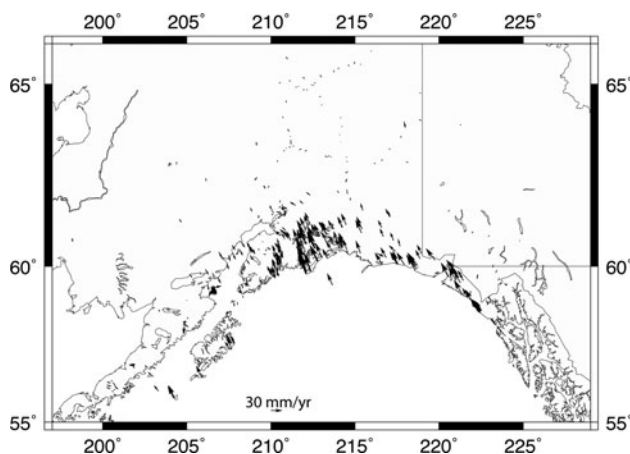


Fig. 8 Residuals calculated using the HTDP3.0 Alaska grid showing the systematic mismatch in coastal Alaska. *Note the scale difference with Fig. 8*

Although there are some outliers to the HTDP 3.1 model, most of the residuals are small and (for the most part) randomly distributed, except between the Kenai Peninsula and Lake Iliamna where the residuals show a consistently northerly trend. This may be caused by the end of the 1998–2001 slow slip event and the gradual decrease in the postseismic relaxation associated with the 1964 Prince William Sound earthquake. Both of these time-dependent effects would be expected to effect the earlier (predominantly campaign) measurements used to develop the grid more than the recent PBO data used in our independent test, which explains why the north bias is visible in the red vectors in Fig. 7 but not the black vectors. Figure 9 shows a histogram of the azimuths of the residuals. Clearly, the azimuths show a peak around the azimuth of zero, which correlates with the northward bias in the residual

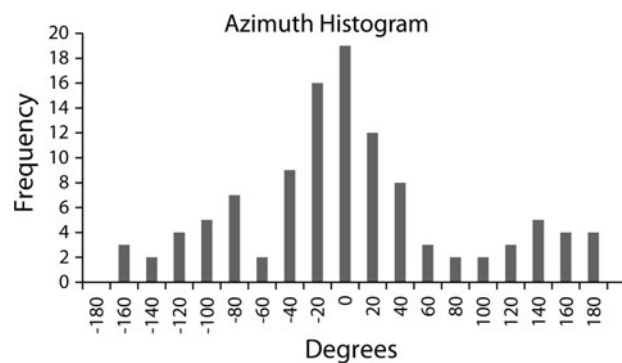


Fig. 9 Histogram of the azimuth of the residual vectors between HTDP 3.1 predicted velocities and measured velocities from the 100 independent test points

Table 5 Statistical summary of test for HTDP 3.1 in Alaska

	Max	Min	RMS	Average
East mm/year	5.62	-5.08	1.661998	-0.47
North mm/year	7.99	-5.51	2.972158	1.39

velocity vectors in the Kenai Peninsula and Lake Iliamna region noted above (Table 5).

The El Mayor–Cucapah earthquake

HTDP 3.1 includes a dislocation model for the M 7.2 El Mayor–Cucapah earthquake that occurred on April 4, 2010 in northern Baja California, Mexico, and is associated with significant deformation south of the of the Salton Sea (see Fig. 10 for location) in Imperial County, California. The dislocation model was developed by Yuri Fialko (2010, personal communication). We tested the model using a set of coseismic displacement vectors derived by Tom Herring at the Massachusetts Institute of Technology (see Fig. 3 of http://www.unavco.org/research_science/science_highlights/2010/M7.2-Baja.html). The displacement vectors are shown in Fig. 10, and the residuals are shown in Fig. 11. Without rejecting any vectors, the RMS of the vector sum of the north and east residuals is only 6.35 mm, and the maximum residuals are approximately 2 cm. Thus, the model governing the El Mayor–Cucapah earthquake seems to fit the observed displacement vectors to within 2.5 cm (Table 6).

Making HTDP more user-friendly

HTDP 3.1 introduces two enhancements that provide people with greater flexibility in using this software, as compared to previous HTDP versions. The first enhancement

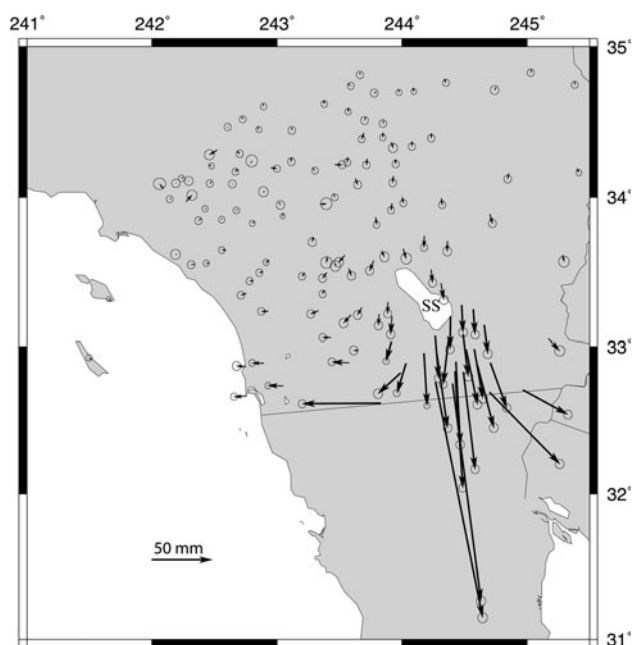


Fig. 10 Displacement vectors associated with the El Mayor–Cucapah earthquake as derived from repeated GPS data in the ITRF2008 reference frame. Error ellipses are shown at the 95% level of confidence. The location of the Salton Sea is labeled by SS

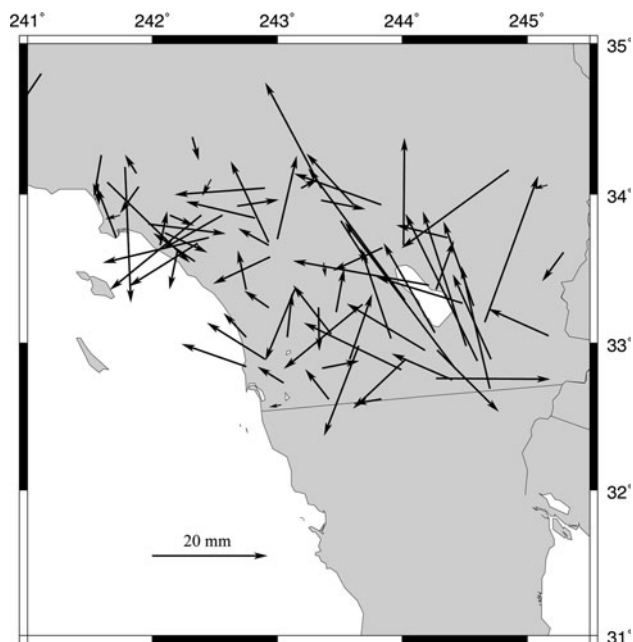


Fig. 11 Residual vectors are relative to ITRF2008 for the displacement vectors from Fig. 10

allows users to submit batch files in a new, convenient format when requesting HTDP services, especially for a large number of geographic points; the second allows users to enter times in the decimal year format, as well as the

Table 6 Statistical summary of test for HTDP 3.1 model of the El Mayor–Cucapah earthquake

	Max (mm)	Min (mm)	RMS (mm)
North resid	24.12	−13.80	3.22
East resid	21.09	−10.79	5.47

traditional month-day-year format. These two enhancements are discussed in the following paragraphs.

HTDP supports five fundamental functions:

- estimate displacements between dates
- estimate crustal velocities
- update positional coordinates and/or geodetic observations to a specified date
- transform positional coordinates between reference frames and/or dates
- transform velocities between reference frames

For each of these functions, HTDP can process several points with geodetic coordinates, together with other metadata, in an electronic ASCII file encoded in the Blue-Book format (Federal Geodetic Control Subcommittee 2000). The Blue-Book format never achieved great popularity; therefore, beginning with version 3.1, users can submit ASCII files in the format to be described later in this section.

With HTDP 3.1, users can submit an ASCII file containing information for multiple locations in a more convenient format. Actually, there are three new formats: one for the first two HTDP functions listed above, one for the third and fourth functions, and one for the fifth function.

For the first two functions (estimating displacements and estimating velocities), each record in the ASCII file must be of the form:

LAT, LON, “TEXT”

where LAT = geodetic latitude in decimal degrees (positive north), LON = longitude in decimal degrees (positive west), and TEXT = descriptive text identifying the point. The descriptive text field can include up to 24 characters between the mandatory quotation marks. The three fields can be separated either by commas or blank spaces, for example,

40.731671553, 112.212671753, “Salt Air”

30.35120.256“Communication tower”

For the third function (updating positional coordinates) and the fourth function (transforming positional coordinates), each record in the input file must be of the form:

LAT, LON, EllipHt, “TEXT”

where EllipHt = ellipsoid height in meters. The other three fields are as previously described.

HTDP can provide updated or transformed 3-D geocentric Cartesian coordinates as well as 3-D geodetic coordinates (geodetic latitude, longitude, and ellipsoid height). The third function also enables users to update geodetic observations such as interstation GPS vectors (GPS baselines), distances, azimuths, and directions. Unfortunately, HTDP 3.1 can only accept values for these observations, together with appropriate metadata, in the Blue-Book format, as is the case with previous HTDP versions.

For the fifth function (transforming velocities between reference frames), each record in the input file must be of the form:

LAT, LON, V_n , V_e , V_u , “TEXT”

where V_n = the north–south component of velocity in mm/year (positive northward), V_e = the east–west component of velocity in mm/year (positive eastward), and V_u = the up–down component of velocity in mm/year (positive upward). The other three fields are as previously described.

As mentioned above, HTDP 3.1 now allows users to enter dates in the decimal year format, which is the format utilized for dates appearing in NGS geodetic control Datasheets and Online Positioning User Service (OPUS) reports. With previous HTDP versions, users could only enter dates in the month–day–year format. Users need to provide dates to HTDP when performing functions 1, 3, and 4.

A date in the decimal year format can be of the form $yyyy.xxx$ where $yyyy$ denotes the year and xxx denotes the fraction of year. Valid examples are

2010.0 for January 1, 2010

1979.359 for May 12, 1979.

The decimal point is required, but the precision is optional. That is, a user may enter $yyyy.$ or $yyyy.xxxxxx$ where any reasonable number of “x” may follow the decimal point. HTDP actually uses the decimal year representation for its internal computations. When a user provides a date in the month–day–year format, HTDP subtracts one from the Julian day number and divides this difference by 365 (or 366 if a leap year) to obtain the fraction of the year. Thus, the computed fraction corresponds to UTC midnight at the beginning of the day.

Conclusions

HTDP 3.1 includes upgraded models of the velocity field for both CONUS and Alaska and a model for the El Mayor–Cucapah earthquake. In particular, the improvement for

Alaska is probably the most important change because the previous velocity model had a significant bias of about 30 mm/year in south-central Alaska. In addition, adding the El Mayor–Cucapah earthquake is important because it is the largest earthquake to affect CONUS since the 1992 M 7.5 Landers earthquake. The El Mayor–Cucapah earthquake is associated with significant deformation in the vicinities of the Salton Sea and the cities of El Centro and Calexico in Imperial County, California. The new velocity grids for CONUS included in this version of HTDP utilize two additional years of PBO data plus velocity vectors derived as part of the Multi-Year CORS reprocessing performed by NGS. HTDP 3.1 shows a small but significant improvement in fit for western CONUS as compared to HTDP 3.0. We also added a smaller-spaced grid to better resolve the velocity variation occurring near the creeping segment of California’s San Andreas fault. HTDP 3.1 also incorporates 14-parameter transformations between ITRF2008 and other popular reference frames. The Appendix presents equations for transforming ITRF2008 coordinates between ITRF2008 and each of three different plate-fixed realizations of the North American Datum of 1983 (NAD 83).

Acknowledgments Rob McCaffrey of Portland State University developed the original DEFNODE model of western CONUS while under contract to the National Geodetic Survey in 2007. We gratefully acknowledge Jeff Freymueller of the University of Alaska, Fairbanks who hosted one of us (Chris Pearson) on two occasions and suggested that we develop the Alaskan deformation model described here. Thanks are also due to Dr. Yuri Fialko of University of California San Diego (UCSD) for making his dislocation model of the El Mayor–Cucapah earthquake available prior to publication. The paper has significantly benefited from reviews by Marti Ikehara, Dave Minkel and Dru Smith of National Geodetic Survey, Duncan Agnew of UCSD and Thomas Meyer of the University of Connecticut.

Appendix: Transforming coordinates between ITRF2008 and NAD 83

This appendix presents equations for transforming positional coordinates between ITRF2008 and NAD 83 (CORS96). We also present equations for transforming positional coordinates between ITRF2008 and NAD 83 (PACP00), as well as equations for transforming positional coordinates between ITRF2008 and NAD 83 (MARP00). These equations were incorporated into HTDP 3.1. In the following text, the names—NAD 83 (CORS96), NAD 83 (PACP00), and NAD 83 (MARP00)—will be truncated to NAD 83 when referring to these three NAD 83 realizations collectively.

Let $x(t)_{\text{NAD 83}}$, $y(t)_{\text{NAD 83}}$ and $z(t)_{\text{NAD 83}}$ denote the NAD 83 positional coordinates for a point at time t as expressed in a 3-D Cartesian earth-centered, earth-fixed coordinate system. These coordinates are expressed as a function of

time to reflect the reality of the crustal motion associated with plate tectonics, land subsidence, volcanic activity, postglacial rebound and so on. Similarly, let $x(t)_{\text{ITRF}}$, $y(t)_{\text{ITRF}}$ and $z(t)_{\text{ITRF}}$ denote the ITRF2008 positional coordinates for this same point at time t . The given ITRF2008 coordinates are related to their corresponding NAD 83 coordinates by a similarity transformation that is approximated by the following equations

$$\begin{aligned}x(t)_{\text{NAD83}} &= T_x(t) + [1 + s(t)] \cdot x(t)_{\text{ITRF}} \\ &\quad + \omega_z(t) \cdot y(t)_{\text{ITRF}} - \omega_y(t) \cdot z(t)_{\text{ITRF}} \\ y(t)_{\text{NAD83}} &= T_y(t) - \omega_z(t) \cdot x(t)_{\text{ITRF}} + [1 + s(t)] \cdot y(t)_{\text{ITRF}} \\ &\quad + \omega_x(t) \cdot z(t)_{\text{ITRF}} \\ z(t)_{\text{NAD83}} &= T_z(t) + \omega_y(t) \cdot x(t)_{\text{ITRF}} - \omega_x(t) \cdot y(t)_{\text{ITRF}} \\ &\quad + [1 + s(t)] \cdot z(t)_{\text{ITRF}}\end{aligned}\quad (1)$$

Here, the symbols $T_x(t)$, $T_y(t)$, and $T_z(t)$ are translations along the x -, y -, and z -axes, respectively; $\omega_x(t)$, $\omega_y(t)$, and $\omega_z(t)$ are counterclockwise rotations about these same three axes; and $s(t)$ is the differential scale change between ITRF2008 and NAD 83. These approximate equations suffice because the three rotations have small magnitudes. Note that each of the seven quantities is represented as a function of time because space-based geodetic techniques have enabled scientists to detect their time-related variations with some degree of accuracy. These time-related variations are assumed to be mostly linear, so that the quantities may be expressed by the following equations,

$$\begin{aligned}T_x(t) &= T_x(t_0) + \dot{T}_x \cdot (t - t_0) \\ T_y(t) &= T_y(t_0) + \dot{T}_y \cdot (t - t_0) \\ T_z(t) &= T_z(t_0) + \dot{T}_z \cdot (t - t_0) \\ \omega_x(t) &= [\varepsilon_x(t_0) + \dot{\varepsilon}_x \cdot (t - t_0)] \cdot m_r \\ \omega_y(t) &= [\varepsilon_y(t_0) + \dot{\varepsilon}_y \cdot (t - t_0)] \cdot m_r \\ \omega_z(t) &= [\varepsilon_z(t_0) + \dot{\varepsilon}_z \cdot (t - t_0)] \cdot m_r \\ s(t) &= s(t_0) + \dot{s} \cdot (t - t_0)\end{aligned}\quad (2)$$

where $m_r = 4.84813681 \cdot 10^{-9}$ is the conversion factor from milliarc seconds (mas) to radians.

Here, the symbol t_0 denotes a fixed, prespecified time of reference. Hence the seven quantities $T_x(t_0)$, $T_y(t_0)$, \dots , $s(t_0)$ are all constants. The seven other quantities \dot{T}_x , \dot{T}_y , \dots , \dot{s} , which represents rates of change with respect to time, are also assumed to be constants.

The transformation from ITRF2008 to NAD 83 (CORS96), denoted (ITRF2008→NAD 83 (CORS96)), is defined in terms of the composition of five distinct transformations, applied sequentially. First, positional coordinates are transformed from ITRF2008 to ITRF2005, then from ITRF2005 to ITRF2000, then from ITRF2000 to ITRF97, then from ITRF97 to ITRF96, and finally from

ITRF96 to NAD 83 (CORS96). This composition may be symbolically expressed via the following equation:

$$\begin{aligned}(\text{ITRF2008} \rightarrow \text{NAD 83 (CORS96)}) &= (\text{ITRF2008} \rightarrow \text{ITRF2005}) \\ &\quad + (\text{ITRF2005} \rightarrow \text{ITRF2000}) + (\text{ITRF2000} \rightarrow \text{ITRF97}) \\ &\quad + (\text{ITRF97} \rightarrow \text{ITRF96}) + (\text{ITRF96} \rightarrow \text{NAD 83 (CORS96)})\end{aligned}\quad (3)$$

where (ITRF2008→ITRF2005) denotes the transformation from ITRF2008 to ITRF2005, (ITRF2005→ITRF2000) denotes the transformation from ITRF2005 to ITRF2000, and so forth.

For (ITRF2008→ITRF2005), HTDP uses the parameter values adopted by the International Earth Rotation and Reference System Service (IERS) for $t_0 = 2005.00$ (~1 January 2005) (Altamimi et al. 2011). We have converted the IERS-adopted values for $t_0 = 2005.00$ to their corresponding values for $t_0 = 1997.00$. Table 7 displays both sets of values.

For (ITRF2005→ITRF2000), HTDP uses the parameters adopted by the IERS for $t_0 = 2000.00$ (Altamimi et al. 2007). The corresponding values for $t_0 = 1997.00$ are given by Pearson et al. (2010).

For (ITRF2000→ITRF97), (ITRF97→ITRF96), and (ITRF96→NAD 83 (CORS96)), HTDP uses the parameter values adopted by NGS for $t_0 = 1997.00$ (Soler and Snay 2004). Table 7 summarizes the values adopted for all transformations at $t_0 = 1997.00$.

Because the values for the parameters associated with each of the five transformations, appearing on the right side of equation (A3), are rather small in magnitude, the values for the parameters of (ITRF2008→NAD 83 (CORS96)) at $t_0 = 1997.00$ may be computed with sufficient accuracy by adding the corresponding values for these five transformations at $t_0 = 1997.00$. The right-most column of Table 7 displays the resulting values used by HTDP. It should be noted that many of the values, given in Table 7, are expressed to more significant digits than the accuracy to which they can be resolved using current geodetic observations. Nevertheless, HTDP uses these values. The inverse transformation (NAD 83 (CORS96)→ITRF2008) at $t_0 = 1997.00$ is obtained by changing the sign for each of the 14 values appearing in the right-most column of Table 7.

Transforming coordinates between ITRF2008 and NAD 83 (PACP00)

Snay (2003) introduced the NAD 83 (PACP00) realization of a Pacific plate-fixed version of the NAD 83 reference frame so that points located in the stable interior of the Pacific tectonic plate would experience little or no

Table 7 Transformation from ITRF2008 to NAD 83 (CORS96)

Parameter	Units	(ITRF2008 → ITRF2005) $t_0 = 2005.00$	(ITRF2008 → ITRF2005) $t_0 = 1997.00$	(ITRF2005 → ITRF2000) $t_0 = 1997.00$	(ITRF2000 → ITRF97) $t_0 = 1997.00$	(ITRF97 → ITRF96) $t_0 = 1997.00$	(ITRF96 → NAD 83) $t_0 = 1997.00$	(ITRF2008 → NAD 83) $t_0 = 1997.00$
Source		Altamimi et al. (2011)	Computed from previous column	Pearson et al. (2010)	Soler and Snay (2004)	Soler and Snay (2004)	Soler and Snay (2004)	Sum of previous five columns
$T_x(t_0)$	m	-0.0005	-0.0029	+0.0007	+0.0067	-0.00207	+0.9910	+0.99343
$T_y(t_0)$	m	-0.0009	-0.0009	-0.0011	+0.0061	-0.00021	-1.9072	-1.90331
$T_z(t_0)$	m	-0.0047	-0.0047	-0.0004	-0.0185	+0.00995	-0.5129	-0.52655
$\epsilon_x(t_0)$	mas	0.000	0.000	0.000	0.000	+0.12467	+25.79	+25.91467
$\epsilon_y(t_0)$	mas	0.000	0.000	0.000	0.000	-0.22355	+9.65	+9.42645
$\epsilon_z(t_0)$	mas	0.000	0.000	0.000	0.000	-0.06065	+11.66	+11.59935
$s(t_0)$	ppb	+0.94	+0.94	+0.16	+1.55	-0.93496	0.00	+1.71504
\dot{T}_x	m/year	+0.0003	+0.0003	-0.0002	0.0000	+0.00069	0.0000	+0.00079
\dot{T}_y	m/year	0.0000	0.0000	+0.0001	-0.0006	-0.00010	0.0000	-0.00060
\dot{T}_z	m/year	0.0000	0.0000	-0.0018	-0.0014	+0.00186	0.0000	-0.00134
$\dot{\epsilon}_x$	mas/year	0.000	0.000	0.000	0.000	+0.01347	+0.0532	+0.06667
$\dot{\epsilon}_y$	mas/year	0.000	0.000	0.000	0.000	-0.01514	-0.7423	-0.75744
$\dot{\epsilon}_z$	mas/year	0.000	0.000	0.000	-0.020	+0.00027	-0.0316	-0.05133
\dot{s}	ppb/year	0.00	0.00	+0.08	+0.01	-0.19201	0.00	-0.10201

Counterclockwise rotations of axes are positive

Table 8 Transformation from ITRF2000 to NAD 83 (PACP00)

Parameter	Units	(ITRF2000→NAD83(PACP00)) $t_0 = 1993.62$	(ITRF2000→NAD83(PACP00)) $t_0 = 1997.00$
Source		Snay (2003)	Computed from previous column
$T_x(t_0)$	m	0.9102	0.9102
$T_y(t_0)$	m	-2.0141	-2.0141
$T_z(t_0)$	m	-0.5602	-0.5602
$\varepsilon_x(t_0)$	mas	29.039	27.741
$\varepsilon_y(t_0)$	mas	10.065	13.469
$\varepsilon_z(t_0)$	mas	10.101	2.712
$s(t_0)$	ppb	0	0
\dot{T}_x	m/year	0	0
\dot{T}_y	m/year	0	0
\dot{T}_z	m/year	0	0
$\dot{\varepsilon}_x$	mas/year	-0.384	-0.384
$\dot{\varepsilon}_y$	mas/year	1.007	1.007
$\dot{\varepsilon}_z$	mas/year	-2.186	-2.186
\dot{s}	ppb/year	0	0

Counterclockwise rotations of axes are positive

Table 9 Transformation from ITRF2008 to NAD 83 (PACP00)

Parameter	Units	(ITRF2008→ITRF2005) $t_0 = 1997.00$	(ITRF2005→ITRF2000) $t_0 = 1997.00$	(ITRF2000→NAD83(PACP00)) $t_0 = 1997.00$	(ITRF2008→NAD83(PACP00)) $t_0 = 1997.00$
Source		Table 7	Pearson et al. (2010)	Table 8	Sum of previous three columns
$T_x(t_0)$	m	-0.0029	0.0007	0.9102	0.908
$T_y(t_0)$	m	-0.0009	-0.0011	-2.0141	-2.0161
$T_z(t_0)$	m	-0.0047	-0.0004	-0.5602	-0.5653
$\varepsilon_x(t_0)$	mas	0	0	27.741	27.741
$\varepsilon_y(t_0)$	mas	0	0	13.469	13.469
$\varepsilon_z(t_0)$	mas	0	0	2.712	2.712
$s(t_0)$	ppb	0.94	0.16	0	1.1
\dot{T}_x	m/year	0.0003	-0.0002	0	0.0001
\dot{T}_y	m/year	0	0.0001	0	0.0001
\dot{T}_z	m/year	0	-0.0018	0	-0.0018
$\dot{\varepsilon}_x$	mas/year	0	0	-0.384	-0.384
$\dot{\varepsilon}_y$	mas/year	0	0	1.007	1.007
$\dot{\varepsilon}_z$	mas/year	0	0	-2.186	-2.186
\dot{s}	ppb/year	0	0.08	0	0.08

Counterclockwise rotations of axes are positive

horizontal motion relative to this frame. NAD 83 (PACP00) is defined in terms of a transformation from ITRF2000 of the form of Equation A2. Adopted values for the parameters of these equations are listed in Table 8 for $t_0 = 1993.62$. Table 8 also presents equivalent values for $t_0 = 1997.00$.

The transformation from ITRF2008 to NAD 83 (PACP00), denoted (ITRF2008→NAD 83 (PACP00)), is defined in terms of the composition of three distinct transformations, applied sequentially. First, positional coordinates are transformed from ITRF2008 to ITRF2005,

then from ITRF2005 to ITRF2000, and then from ITRF2000 to NAD 83 (PACP00). This composition may be symbolically expressed via the equation

$$\begin{aligned} (\text{ITRF2008} \rightarrow \text{NAD 83(PACP00)}) &= (\text{ITRF2008} \rightarrow \text{ITRF2005}) \\ &+ (\text{ITRF2005} \rightarrow \text{ITRF2000}) + (\text{ITRF2000} \rightarrow \text{NAD 83(PACP00)}) \end{aligned} \quad (4)$$

Table 9 displays values for the various parameters at $t_0 = 1997.00$, where values for the transformation from ITRF2005 to ITRF2000 for $t_0 = 1997.00$ were computed by Pearson et al. (2010) from those published by Altamimi

Table 10 Transformation from ITRF2000 to NAD 83 (MARPO0)

Parameter	Units	(ITRF2000→NAD83(MARP00)) $t_0 = 1993.62$	(ITRF2000→NAD83(MARP00)) $t_0 = 1997.00$
Source		Snay (2003)	Computed from previous column
$T_x(t_0)$	m	0.9102	0.9102
$T_y(t_0)$	m	-2.0141	-2.0141
$T_z(t_0)$	meters	-0.5602	-0.5602
$\epsilon_x(t_0)$	mas	29.039	28.971
$\epsilon_y(t_0)$	mas	10.065	10.42
$\epsilon_z(t_0)$	mas	10.101	8.928
$s(t_0)$	ppb	0	0
\dot{T}_x	m/year	0	0
\dot{T}_y	m/year	0	0
\dot{T}_z	m/year	0	0
$\dot{\epsilon}_x$	mas/year	-0.02	-0.02
$\dot{\epsilon}_y$	mas/year	0.105	0.105
$\dot{\epsilon}_z$	mas/year	-0.347	-0.347
\dot{s}	ppb/year	0	0

Counterclockwise rotations of axes are positive

Table 11 Transformation from ITRF2008 to NAD 83 (MARPO0)

Parameter	Units	(ITRF2008→ITRF2005) $t_0 = 1997.00$	(ITRF2005→ITRF2000) $t_0 = 1997.00$	(ITRF2000→NAD83(MARP00)) $t_0 = 1997.00$	(ITRF2008→NAD83(MARP00)) $t_0 = 1997.00$
Source		Table 7	Pearson et al. (2010)	Table 10	Sum of previous three columns
$T_x(t_0)$	m	-0.0029	0.0007	0.9102	0.908
$T_y(t_0)$	m	-0.0009	-0.0011	-2.0141	-2.0161
$T_z(t_0)$	m	-0.0047	-0.0004	-0.5602	-0.5653
$\epsilon_x(t_0)$	mas	0	0	28.971	28.971
$\epsilon_y(t_0)$	mas	0	0	10.42	10.42
$\epsilon_z(t_0)$	mas	0	0	8.928	8.928
$s(t_0)$	ppb	0.94	0.16	0	1.1
\dot{T}_x	m/year	0.0003	-0.0002	0	0.0001
\dot{T}_y	m/year	0	0.0001	0	0.0001
\dot{T}_z	m/year	0	-0.0018	0	-0.0018
$\dot{\epsilon}_x$	mas/year	0	0	-0.02	-0.02
$\dot{\epsilon}_y$	mas/year	0	0	0.105	0.105
$\dot{\epsilon}_z$	mas/year	0	0	-0.347	-0.347
\dot{s}	ppb/year	0	0.08	0	0.08

Counterclockwise rotations of axes are positive

et al. (2007) for $t_0 = 2000.00$. The right-most column in this table is obtained by adding the previous three columns across each row.

Transforming coordinates between ITRF2008 and NAD 83 (MARPO0)

Snay (2003) introduced the NAD 83 (MARPO0) realization of a Mariana plate-fixed version of the NAD 83 reference frame so that points located on the Marianna tectonic plate

would experience little or no horizontal motion relative to this frame. NAD 83 (MARPO0) is defined in terms of a transformation from ITRF2000 of the form of Equation A2. Adopted values for the parameters of these equations are listed in Table 10 for $t_0 = 1993.62$. Table 10 also presents equivalent values for $t_0 = 1997.00$.

The transformation from ITRF2008 to NAD 83 (MARPO0) is defined in terms of the composition of three distinct transformations, applied sequentially. First, positional coordinates are transformed from ITRF2008 to ITRF2005, then from ITRF2005 to ITRF2000, and then

from ITRF2000 to NAD 83 (MARP00). This composition may be symbolically expressed via the equation

$$\begin{aligned} (\text{ITRF2008} \rightarrow \text{NAD 83(MARP00)}) &= (\text{ITRF2008} \rightarrow \text{ITRF2005}) \\ &+ (\text{ITRF2005} \rightarrow \text{ITRF2000}) + (\text{ITRF2000} \rightarrow \text{NAD 83(MARP00)}) \end{aligned} \quad (5)$$

Table 11 displays values for the various parameters at $t_0 = 1997.00$. The right-most column in this table is obtained by adding the previous three columns across each row.

Related transformations

The International GNSS Service(IGS) recently adopted a reference frame called IGS08 that is based on ITRF2008. IGS08 coordinates for some reference stations differ from their corresponding ITRF2008 coordinates because the IGS08 coordinates were computed using more current calibrations of GPS antennas than were used in computing ITRF2008 coordinates. Nevertheless, IGS considers the 14-parameter transformation between ITRF2008 and IGS08 to be the identity function, that is, each of the 14 transformation parameters is zero in value. As a result, the value of the 14 parameters in the transformation between IGS08 and a given NAD 83 realization is the same as the values of the 14 parameters in the corresponding transformation between ITRF2008 and this NAD 83 realization.

Also, NGS recently adopted three new reference frames called NAD 83 (2011), NAD 83 (PA11), and NAD 83 (MA11). To create these reference frames, NGS reprocessed its collection of GPS data from the CORS network to compute IGS08 coordinates for reference stations in this network. The corresponding NAD 83 (2011) coordinates were then obtained by applying the (ITRF2008 \rightarrow NAD 83 (CORS96)) transformation given in this paper, which as mentioned above is the same as the (IGS08 \rightarrow NAD 83 (CORS96)) transformation. As a result, the 14-parameter transformation between NAD 83 (CORS96) and NAD 83 (2011) is the identity function. In most cases, NAD 83 (CORS96) coordinates for a given reference station will differ from the corresponding NAD 83 (2011) coordinates for this same reference frame because the NAD 83 (2011) coordinates were computed using more GPS data, more recent models for systematic errors (like ocean loading), and improved mathematical algorithms than were involved in the NAD 83 (CORS96) computations many of which were performed in 2002. Thus, the fact that the 14-parameter transformation between two reference frames is the identity function does not mean that corresponding coordinates in the two frames agree exactly in value. It only means that these corresponding coordinates agree on average when considering all the reference stations in the network, which have coordinates in both reference frames.

In the same manner, the transformation between ITRF2008 (or IGS08) and NAD 83 (PA11) is the same as the transformation between ITRF2008 and NAD 83 (PACP00), and the transformation between ITRF2008 and NAD 83 (MA11) is the same as the transformation between ITRF2008 and NAD 83 (MARP00). Thus, the transformation between NAD 83 (PA11) and NAD 83 (PACP00) is the identity function, and the transformation between NAD 83 (MA11) and NAD 83 (MARP00) is also the identity function.

References

- Altamimi Z, Collilieux X, Legrand J, Garayt B, Boucher C (2007) ITRF2005: a new release of the International Terrestrial Reference Frame based on time series of station positions and Earth orientation parameters. *J Geophys Res.* doi:[10.1029/2007JB004949](https://doi.org/10.1029/2007JB004949)
- Altamimi Z, Collilieux X, Metivier L (2011) ITRF2008: an improved solution of the international terrestrial reference frame. *J Geod.* doi:[10.1007/s00190-011-0444-4](https://doi.org/10.1007/s00190-011-0444-4)
- Cross R, Freymueller JT (2007) Plate coupling variation and block translation in the Andreanof segment of the Aleutian arc determined by subduction zone modeling using GPS data. *Geophys Res Lett.* doi:[10.1029/2006GL029073R](https://doi.org/10.1029/2006GL029073R)
- Cross R, Freymueller JT (2008) Evidence for and implications of a Bering plate based on geodetic measurements from the Aleutians and western Alaska. *J Geophys Res.* doi:[10.1029/2007JB005136](https://doi.org/10.1029/2007JB005136)
- D'Alessio MA, Johanson IA, Bürn, Schmidt DA, Murray MH (2005) Slicing up the San Francisco Bay area: block kinematics and fault slip rates from GPS-derived surface velocities. *J Geophys Res.* doi:[10.1029/2004JB003496](https://doi.org/10.1029/2004JB003496)
- Dixon T, Decaix J, Farina F, Furlong K, Malservisi R, Bennett R, Suarez-Vidal F, Fletcher J, Lee J (2002) Seismic cycle and rheological effects on estimation of present-day slip rates for the Agua Blanca and San Miguel-Vallecitos faults, northern Baja California, Mexico. *J Geophys Res.* doi:[10.1029/2000JB000099](https://doi.org/10.1029/2000JB000099)
- Elliott JL, Larsen CF, Freymueller JT, Motyka RJ (2010) Tectonic block motion and glacial isostatic adjustment in southeast Alaska and adjacent Canada constrained by GPS measurements. *J Geophys Res.* doi:[10.1029/2009JB007139](https://doi.org/10.1029/2009JB007139)
- Federal Geodetic Control Subcommittee (2000) Input formats and specifications of the National Geodetic Survey Data Base the NGS "Bluebook" <http://www.ngs.noaa.gov/FGCS/BlueBook/>. Accessed 26 July 2011
- Freymueller JT, Cohen SC, Cross R, Elliott J, Fletcher H, Larsen C, Hreinsdóttir S, Zweck C (2008) Active deformation processes in Alaska, based on 15 years of GPS measurements. In: Freymueller JT et al (eds) *Active tectonics and seismic potential of Alaska*. AGU, Washington, DC, pp 1–42
- Hammond WC, Thatcher W (2004) Contemporary tectonic deformation of the basin and range province, western United States: 10 years of observation with the Global Positioning System. *J Geophys Res.* doi:[10.1029/2003JB002746](https://doi.org/10.1029/2003JB002746)
- Hammond WC, Thatcher W (2005) Northwest basin and range tectonic deformation observed with the Global Positioning System. *J Geophys Res.* doi:[10.1029/2005JB003678](https://doi.org/10.1029/2005JB003678)
- King NE, Argus D, Langbein J, Agnew DC, Bawden G, Dollar RS, Liu Z, Galloway D, Reichard E, Yong A, Webb FH, Bock Y, Stark K, Barseghian D (2007) Space geodetic observation of expansion of the San Gabriel Valley, California, aquifer system,

- during heavy rainfall in winter 2004–2005. *J Geophys Res.* doi: [10.1029/2006JB0044](https://doi.org/10.1029/2006JB0044)
- Marquez-Azua B, DeMets C (2003) Crustal velocity field of Mexico from continuous GPS measurements, 1993 to June 2001: implications for neotectonics of Mexico. *J Geophys Res.* doi: [10.1029/2002JB002241](https://doi.org/10.1029/2002JB002241)
- McCaffrey R (1995) “DEFNODE users’ guide” Rensselaer Polytechnic Institute, Troy, New York. <http://www.rpi.edu/~mccaffr/defnode/>. Accessed 8 Mar 2007
- McCaffrey R (2002) Crustal block rotations and plate coupling. In: Stein S, Freymueller J (eds), *Plate boundary zones*. AGU Geodynamics Series 30, pp 101–122
- McCaffrey R (2005) Block kinematics of the Pacific/North America plate boundary in the southwestern United States from inversion of GPS, seismological, and geologic data. *J Geophys Res.* doi: [10.1029/2004JB003307](https://doi.org/10.1029/2004JB003307)
- McCaffrey R, Qamar AI, King RW, Wells R, Ning Z, Williams CA, Stevens CW, Vollick JJ, Zwick PC (2007) Plate locking, block rotation and crustal deformation in the Pacific Northwest. *Geophys J Int.* doi: [10.1111/j.1365-264X.2007.03371.x](https://doi.org/10.1111/j.1365-264X.2007.03371.x)
- Payne SJ, McCaffrey R, King RW (2007) Contemporary deformation within the Snake River Plain and northern basin and range province, USA. *EOS Trans Am Geophys Union* 88(23):T22A-05
- Pearson C, McCaffrey R, Elliott JL, Snay R (2010) HTDP 3.0: software for coping with coordinate changes associated with crustal motion. *J Surv Eng* 136:80–90. doi: [10.1061/\(ASCE\)SU.1943-5428.0000013](https://doi.org/10.1061/(ASCE)SU.1943-5428.0000013)
- Sella GF, Stein S, Dixon TH, Craymer M, James TS, Mazzotti S, Dokka RK (2007) Observation of glacial isostatic adjustment in “stable” North America with GPS. *Geophys Res Lett.* doi: [10.1029/2006GL027081](https://doi.org/10.1029/2006GL027081)
- Shen ZK, King RW, Agnew DC, Wang M, Herring TA, Dong S, Fang P (2011) A unified analysis of crustal motion in southern California, 1970–2004: the SCEC crustal motion map. *J Geophys Res* 116 (in press)
- Snay RA (2003) Introducing two spatial reference frames for regions of the Pacific Ocean. *Surv Land Inf Sci* 63:5–12
- Soler T, Snay RA (2004) Transforming positions and velocities between the International Terrestrial Reference Frame of 2000 and North American Datum of 1983. *J Surv Eng* 130:49–55. doi: [10.1061/\(ASCE\)0733-9453\(2004\)130:2\(49\)](https://doi.org/10.1061/(ASCE)0733-9453(2004)130:2(49))
- Suito H, Freymueller JT (2009) A viscoelastic and afterslip post-seismic deformation model for the 1964 Alaska earthquake. *J Geophys Res.* doi: [10.1029/2008JB005954](https://doi.org/10.1029/2008JB005954)
- Williams TB, Kelsey HM, Freymueller JT (2006) GPS-derived strain in northwestern California: termination of the San Andreas fault system and convergence of the Sierra Nevada-Great Valley block contribution to southern Cascadia forearc contraction. *Tectonophysics* 413:171–184

Author Biographies

Chris Pearson works for the National Geodetic Survey where he is the geodetic advisor for Illinois. He is also responsible for maintaining the model of crustal deformation that NGS uses to correct coordinates and survey data for tectonic motion in the western US.

Richard Snay served as a scientist with the U.S. National Geodetic Survey (NGS) from 1974 to 2010. Dr. Snay managed the U.S. Continuously Operating Reference Station (CORS) program from 1998 to 2007, and he supervised NGS’ Spatial Reference System Division from 2003 to 2010.